

Secondary ion yield changes on rippled interfaces

Maxim A. Makeev and Albert-László Barabási^{a)}

Department of Physics, University of Notre Dame, Notre Dame, Indiana 46556

(Received 30 October 1997; accepted for publication 22 December 1997)

Sputter erosion often leads to the development of surface ripples. Here we investigate the effect of the ripples on the secondary ion yield, by calculating the yield as a function of the microscopic parameters characterizing the ion cascade (such as penetration depth, widths of the deposited energy distribution) and the ripples (ripple amplitude, wavelength). We find that ripples can strongly enhance the yield, with the magnitude of the effect depending on the interplay between the ion and ripple characteristics. Furthermore, we compare our predictions with existing experimental results. © 1998 American Institute of Physics. [S0003-6951(98)03108-8]

Ripple formation during ion bombardment has been observed for various bombarding ions and substrates, under a wide range of sputtering conditions (such as ion energy and angle of incidence).^{1–8} The numerous experimental studies have motivated theoretical investigations of the basic mechanisms responsible for the formation and evolution of ripples.^{5–7} On the other hand, less attention has been paid to the effect of the ripples on the sputtering yield. The classical literature on ion sputtering yield uses the *flat surface approximation*, thus ignoring the surface topography.^{9–11} Although experiments have shown that the surface topography modifies the sputtering yield,^{12–14} there is no theory which would account for this effect.

In this letter we investigate the influence of the surface ripples on the secondary ion yields. We calculate the yield as a function of the parameters characterizing the ripple structure, finding that the nonplanar morphology can strongly *enhance* the yield, depending on the interplay between the ripple and the incident ion parameters. In particular, we show that the flat-surface approximation strongly underestimates the yield, since the topography induced yield increase can be as large as 100%. Finally we compare our predictions with experimental results on the secondary ion yield changes on rippled interfaces.

The physical process which takes place during ion bombardment is illustrated in Fig. 1. We choose the local system of coordinates in which z' is parallel to the direction of the incident ions and x', y' are located in the plane perpendicular to it. An ion strikes the surface at point A, and stops at a distance a , at point P, with coordinates (x', y', z') , after all its energy is dissipated due to elastic and nonelastic interactions with the atoms of the material. According to Sigmund¹¹ the energy deposited by the ion at point A with coordinates $(0,0,0)$ is given by the Gaussian

$$E(r'_\perp, z') = \frac{\epsilon}{(2\pi)^{3/2} \sigma \mu^2} \exp\left(-\frac{z'^2}{2\sigma^2} - \frac{x'^2 + y'^2}{2\mu^2}\right), \quad (1)$$

where ϵ is the total energy of an incident ion and σ and μ are the widths of the deposited energy distribution along z' and x' (y') directions, respectively. Since there are many ions reaching the surface simultaneously, the erosion rate or the

surface velocity at point A, proportional to the energy deposited by the bombarding ions, is an integral over all points R at which ions stop in the bulk

$$v = p \int_R d\mathbf{r}'_\perp E[\mathbf{r}'_\perp, z'(x', y')] \Phi(x'). \quad (2)$$

Here $p = 3/(4\pi^2 n^2 U_0 C_0)$,¹¹ where n is a density of a target atoms, U_0 is the surface binding energy and C_0 is a constant proportional to the square of effective radius of the interatomic interaction potential. The $\Phi(x')$ is a local correction to the uniform flux f .⁶ From Eq. (2) we can calculate the yield using¹¹

$$Y = \frac{vn}{\bar{f}}, \quad (3)$$

where the flux corrected for the local slope has the form $\Phi(x') = f \cos\{\arctan(\partial z'/\partial x')\}$ and \bar{f} is averaged over the period of ripple modulations flux; $\bar{f} = \langle \Phi(x') \rangle$. Neglecting the fluctuations in the shape of the ripples, the ripple structure with amplitude h_0 can be approximated by the height function

$$h(x) = h_0 \cos(2\pi x/\lambda). \quad (4)$$

Performing the integral over y' and taking the average over y'_0 we obtain the expression for the total yield at an arbitrary point x'_0 along the surface, measured in the local coordinate frame as

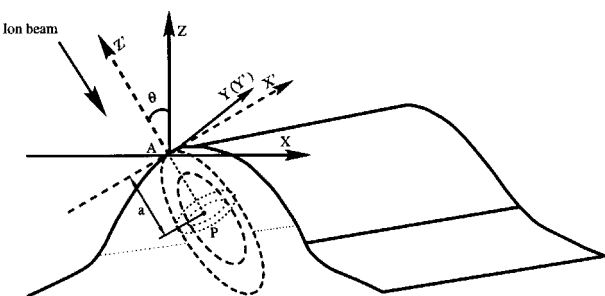


FIG. 1. Following a straight trajectory (solid line) the ion penetrates an average distance a inside the solid (dotted line) after which it completely spreads out its kinetic energy. The energy decreases with the distance from P , the dotted curves indicating schematically the equal energy contours. The energy released at point P contributes to erosion at A.

^{a)}Electronic mail: alb@nd.edu

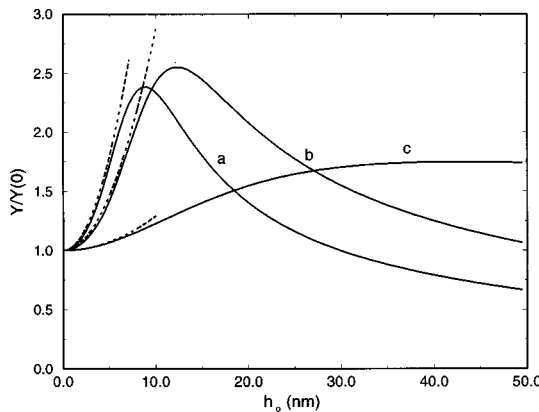


FIG. 2. Normalized yield vs amplitude of the periodic modulation plotted for fixed values of $\lambda=500 \text{ \AA}$ and $a=50 \text{ \AA}$, and different angles of incidence: (A) $\theta=45^\circ$; (b) $\theta=35^\circ$; (c) $\theta=0^\circ$. Dashed lines represent the small h_0/a expansion for (a), (b), (c), respectively.

$$Y(x'_0) = \frac{pn\epsilon}{(2\pi)\mu\sigma\bar{f}} \int_{-\infty}^{\infty} dx \Phi(x') \times \exp \left\{ -\frac{(a-[z'(x')-z'(x'_0)])^2}{2\sigma^2} - \frac{(x'-x'_0)^2}{2\mu^2} \right\}. \quad (5)$$

To proceed further we need to transform the coordinate system from the *local* to the *laboratory* frame with the z axis perpendicular to the average surface orientation. If the angle of incidence of the primary ions with respect to the z axis is θ , such a transformation is a simple rotation in the $z-x$ plane. Finally, in order to obtain the average yield we have to average Eq. (5) over the period of modulation

$$Y = \frac{1}{\lambda} \int_0^\lambda dx_0 Y(x_0). \quad (6)$$

Combining Eqs. (2)–(6) we obtain the following expression for the average yield:

$$Y = F \exp(-1/2\epsilon_1^2) \int_0^\lambda \int_{-\infty}^{\infty} dx dx_0 \cos \left\{ \arctan \left[\theta - \left(\frac{\partial h}{\partial x} \right) \right] \right\} \times \exp \left\{ -\frac{\Gamma_1(x-x_0)^2}{a^2} \right\} \times \exp \left\{ -\frac{\Gamma_2[h(x)-h(x_0)]^2}{a^2} \right\} \times \exp \left\{ -\frac{\Gamma_3(x-x_0)[h(x)-h(x_0)]}{a^2} \right\} \times \exp \left\{ -\frac{\Gamma_4(x-x_0)}{a^2} \right\} \exp \left\{ -\frac{\Gamma_5[h(x)-h(x_0)]}{a^2} \right\}, \quad (7)$$

where $F=(pn\epsilon)/(2\pi\mu\sigma\bar{f})$, $\Gamma_{1,2}=\sin(\theta)^2/2\epsilon_{1,2}^2 + \cos(\theta)^2/2\epsilon_{2,1}^2$, $\Gamma_3=(1/\epsilon_2^2-1/\epsilon_1^2)\sin(\theta)\cos(\theta)$, $\Gamma_4=(1/\epsilon_1^2)\sin(\theta)$, $\Gamma_5=-(1/\epsilon_1^2)\cos(\theta)$, and \bar{f} is the average flux, given by

$$\bar{f}=f \int_0^\infty dx \cos \left\{ \theta - \arctan \left[\left(\frac{2\pi h_0}{\lambda} \right) \sin \left(\frac{2\pi x}{\lambda} \right) \right] \right\}. \quad (8)$$

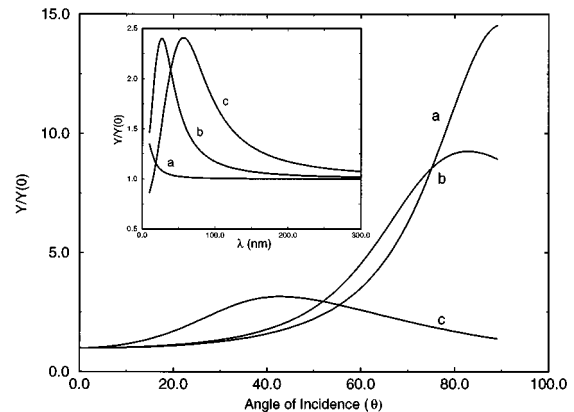


FIG. 3. Normalized yield vs angle of incidence for different amplitudes of the periodic modulation plotted for fixed value of $\lambda=2000 \text{ \AA}$, and $a=50 \text{ \AA}$; (a) $h_0=0 \text{ \AA}$; (b) $h_0=100 \text{ \AA}$; (c) $h_0=500 \text{ \AA}$. The inset shows the yield vs wavelength of the ripples for fixed value of the penetration depth, $a=50 \text{ \AA}$ and $\theta=45^\circ$. Different curves correspond to: (a) $h_0=10 \text{ \AA}$; (b) $h_0=50 \text{ \AA}$; and (c) $h_0=100 \text{ \AA}$.

To account for the secondary ion yield changes due to the ripple structure we integrate Eqs. (7)–(8) numerically for h_0 spanning the region from 0 to 500 \AA , corresponding to the experimentally relevant parameter range. We use $\epsilon_1=1/2$ and $\epsilon_2=1/4$, which correspond to the asymmetric energy distribution with $\sigma=a/2$ and $\mu=a/4$. Figure 2 shows the total yield as a function of h_0 for different values of the incident angle θ . As a general tendency, one can see that there is a fast increase in Y for small h_0 . Indeed, next we show that *for small h_0 the yield increase is proportional to h_0^2* . Experiments on ripple formation indicate that the ratio of the height and ripple wavelength is a very small quantity.^{14,15} Consequently, we can expand Eq. (8) in powers of the small parameter $\partial h/\partial x \sim h_0/\lambda$ and keep only terms up to the second order, obtaining the average flux as

$$\bar{f}=f \cos(\theta) \left\{ 1 - \frac{1}{4} \left\{ \frac{2\pi h_0}{\lambda} \right\}^2 \right\}.$$

Although the experimentally relevant range for the amplitude of the ripple height modulations can be much larger than the penetration depth a , at the initial stages of ripple formation h_0/a is a small quantity. Thus we can further expand Eq. (7) in powers of h_0/a obtaining the yield as

$$Y = F \exp \left\{ -\frac{1}{2\epsilon_1^2} \right\} \exp \left\{ \frac{\Gamma_4^2}{4\Gamma_1} \right\} \sqrt{\frac{\pi}{\Gamma_1}} \{ 1 + h_0^2 Y_1 \}, \quad (9)$$

where Y_1 is a parameter independent of h_0 .¹⁶ Equation (9) quantifies the fast increase in Y with h_0 for the early stages of the ripple formation process, predicting that $Y=C_1+C_2 h_0^2+O(h_0^4)$. The dotted lines shown in Fig. 2 indicate that Eq. (9) indeed provides an excellent *parameter free* fit for small h_0 . However, for h_0 comparable to λ the yield decreases with h_0 , and for large h_0 the yield is suppressed by the ripples, decreasing below the value for the flat surface (see the $\theta=45^\circ$ curve in Fig. 2). The explanation of this behavior can be given in terms of local angle variation of the intensity.¹² The detailed discussion regarding the variation of yield from surfaces with particular topography will be given elsewhere.^{16,17}

The inset of Fig. 3 shows the dependence of the yield on

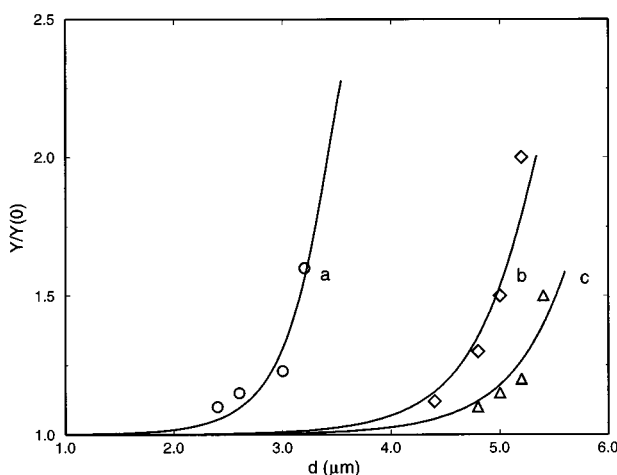


FIG. 4. Normalized yield vs sputtered depth plotted for different values of the incident ion energy and fixed angle of incidence $\theta=40$. The curves correspond to: (a) $a=47 \text{ \AA}$, $\lambda=1980 \text{ \AA}$, $r=1.36 \mu\text{m}^{-1}$; (b) $a=68 \text{ \AA}$, $\lambda=3020 \text{ \AA}$, $r=0.95 \mu\text{m}^{-1}$; (c) $a=100 \text{ \AA}$, $\lambda=4080 \text{ \AA}$, $r=0.91 \mu\text{m}^{-1}$. The circles, diamonds, and triangles correspond to the experimental result for the same values of experimental parameters taken from Ref. 14.

the ripple wavelength for fixed a and h_0 . For $h_0 < a$ the yield monotonically decreases with λ , while it has a maximum for $h_0 \geq a$. In each case the yield approaches the flat surface limit for large λ . Figure 3 shows the yield dependence on the angle of incidence θ . The range of angles close to 90° cannot be accounted for in the framework of this model.⁵ We find that the obtained θ dependence is in qualitative agreement with experimental results by Wittmaak *et al.*¹²

To provide a direct comparison with experiments we plot the yield as a function of sputtered depth for the experimental parameters provided by Vajo *et al.*¹⁴ The yield was normalized to the yield for a flat surface, $Y(0)$. Using Fig. 1 of Ref. 14 we plot the experimental points for the normalized yield enhancement with sputtered depth for 3, 5, 9 keV O₂⁺ sputtering of Si. The linear theory⁵ predicts that in the early stages of ripple formation $h_0 = h_i \exp(rd)$, allowing one to convert h_0 into the sputtered depth d measured experimentally. However, since the experiments indicate that λ is constant only for $d < d_T$, where d_T is an experimentally determined transition depth,¹⁴ we have chosen to fit the experimental data only in this regime. As Fig. 4 demonstrates, using the experimentally determined parameters, Eq. (7) provides an excellent fit to the experimental results.

Other aspects of the experimental results also agree with our predictions. First, by increasing the flux, the yield in-

creases linearly and, indeed, Y in Eq. (7) is proportional to J . Second, the change in the flux doesn't affect the shape of the yield curve, as expected from our theory. Finally, the theory proposed by Wittmaak,¹² that accounts for the change in the yield based on the dependence of the yield on the local slopes, can be derived from our theory. However, our approach provides a more detailed description and is based solely on the *microscopic parameters* characterizing the ion cascade. These results have a potential to greatly enhance our understanding of morphology induced yield modifications, consequently leading to a better use and understanding of such surface characterization techniques as secondary ion mass spectrometry (SIMS).

This research was partially supported by the Faculty Research Program of the University of Notre Dame.

¹S. W. MacLaren, J. E. Baker, N. L. Finnegan, and C. M. Loxton, *J. Vac. Sci. Technol. A* **10**, 468 (1992).

²H. Shichi, K. Ohnishi, and S. Nomura, *Jpn. J. Appl. Phys., Part 2* **30**, L927 (1991); S. Dunkan, R. Smith, D. E. Sykes, and J. M. Walls, *Vacuum* **34**, 145 (1984).

³M. A. Makeev and A.-L. Barabási, *Appl. Phys. Lett.* **71**, 2800 (1997); R. Cuerno, H. A. Makse, S. Tomassone, S. T. Harrington, and H. E. Stanley, *Phys. Rev. Lett.* **75**, 4464 (1995).

⁴E. Chason, T. M. Mayer, B. K. Kellerman, D. N. McIlroy, and A. J. Howard, *Phys. Rev. Lett.* **72**, 3040 (1994); T. M. Mayer, E. Chason, and A. J. Howard, *J. Appl. Phys.* **76**, 1633 (1994).

⁵R. M. Bradley and J. M. E. Harper, *J. Vac. Sci. Technol. A* **6**, 2390 (1988).

⁶R. Cuerno and A.-L. Barabási, *Phys. Rev. Lett.* **74**, 4746 (1995); A.-L. Barabási, M. A. Makeev, C.-S. Lee, and R. Cuerno, in *Dynamics of Fluctuating Interfaces and Related Phenomena*, edited by D. Kim, H. Park, and B. Kahng (World Scientific, Singapore, 1997).

⁷R. M. Bradley, *Phys. Rev. E* **54**, 6149 (1996).

⁸A. Crespo-Sosa, P. Schaaf, W. Bolse, K.-P. Lieb, M. Gimbel, U. Geyer, and C. Tosello, *Phys. Rev. B* **53**, 14795 (1996).

⁹*Sputtering by Particle Bombardment*, edited by R. Behrisch (Springer, Heidelberg, 1981, 1983), Vols. I, II, III; P. D. Townsend, J. C. Kelly, and N. E. W. Hartley, *Ion Implantation, Sputtering and their Applications* (Academic, London, 1976).

¹⁰For overview on surface morphologies see: A.-L. Barabási and H. E. Stanley, *Fractal Concepts in Surface Growth* (Cambridge University Press, Cambridge, 1995).

¹¹P. Sigmund, *Phys. Rev.* **184**, 383 (1969); *J. Mater. Sci.* **8**, 1545 (1973).

¹²K. Wittmaack, *J. Vac. Sci. Technol. A* **8**, 2246 (1990).

¹³F. A. Stevie, P. M. Kahora, D. S. Simons, and P. Chi, *J. Vac. Sci. Technol. A* **6**, 76 (1988).

¹⁴J. J. Vajo, R. E. Doty, and E.-H. Cirlin, *J. Vac. Sci. Technol. A* **14**, 2709 (1996).

¹⁵A. Karen, K. Okuno, F. Soeda, and A. Ishitani, *J. Vac. Sci. Technol. A* **8**, 2247 (1991).

¹⁶M. A. Makeev and A.-L. Barabási (unpublished).

¹⁷Note that for large h_0 redeposition of the sputtered material might further decrease the effective yield. Redeposition is not relevant for small h_0/λ , i.e., when $\partial_x h \ll \theta$.